





Bioavailable strontium isoscape for the Amazon region using tree wood

LA Martinelli^a, CP Bataille^b, AC Batista^{a,*}, IM Souza-Silva^a, MG Araújo^a,
AL Abdalla Filho^a, A. Brunello^a, M. Tommasiello Filho^c, N. Higuchi^d, AC Barbosa^e,
F. Costa^f, GB Nardoto^g

^a Center for Nuclear Energy in Agriculture, University of São Paulo, Av. Centenário 303, Piracicaba, São Paulo CEP 13416-000, Brazil

^b Department of Earth and Environmental Sciences, University of Ottawa, STEM Complex 150, Louis – Pasteur Private, Ottawa, ON K1N 6N5, Canada

^c Department Forest Sciences, Luiz de Queiroz College of Agriculture, University of São Paulo, Av. Pádua Dias, 11, Piracicaba, São Paulo CEP 13418-900, Brazil

^d National Institute for Amazon Research, Av. André Araújo, 2936, Petrópolis, Manaus, Amazonas CEP 69067-375, Brazil

^e Department of Forest Sciences, University of Lavras, P.O.Box 3037, Lavras, Minas Gerais CEP 37200-000, Brazil

^f Instituto Nacional de Criminalística, Polícia Federal, Setor Policial Sul, Lote 7, Asa Sul, Brasília, Distrito Federal CEP 70610-902, Brazil

^g Department of Ecology, Institute of Biological Sciences, University of Brasília, Campus Universitário Darcy Ribeiro Bloco E s/n, Brasília, Distrito Federal CEP 70910-900, Brazil

ARTICLE INFO

Keywords:

Geospatial isoscapes
Illegal logging
Provenance studies
Strontium isotopes

ABSTRACT

Illegal logging is a major environmental crime in the Amazon, driven by organized networks and causing severe ecological and economic impacts. Existing documentation systems, like Brazil's "Forest Origin Document" (DOF), remain vulnerable to fraud, highlighting need for more reliable timber tracking methods. The isotopic composition of strontium ($^{87}\text{Sr}/^{86}\text{Sr}$) in wood has emerged as a promising tool for determining timber provenance. This study developed bioavailable Sr isoscapes for the Amazon using regression kriging and random forest to map $^{87}\text{Sr}/^{86}\text{Sr}$ ratios in tree wood. Wood samples from 67 trees across 21 sites were collected in collaboration with regional institutions. The observed $^{87}\text{Sr}/^{86}\text{Sr}$ range in plant exceeds previously reported global values, showing a strong contrast between the Amazon Trough and Precambrian Shields. Despite the limited dataset, both modeling approaches performed well, producing similar isoscapes and demonstrating that $^{87}\text{Sr}/^{86}\text{Sr}$ ratios in wood are highly predictable and geology – dependent. However, high intra - site variability in Precambrian cratons and limited differentiation across the Amazon highlight the need for additional sampling. The finding confirm the potential of Sr isoscapes to trace timber origin and combat illegal logging. While the models show strong predictive power in some regions, addressing current limitations through expanded sampling will improve accuracy. Future research can refine Sr isoscapes, enhancing their application in law enforcement and sustainable Amazon resource management.

1. Introduction

Illegal logging has become a transnational crime involving numerous actors and highly organized criminal networks. These operations generate vast sums of money that must be laundered, further fueling fraud and corruption (FATF, 2021; Interpol, 2019). The global nature of this illicit activity prompted transboundary organizations, such as the United Nations Office on Drugs and Crime (UNODC), to intervene in 2013. As part of these coordinated efforts, in May 2014, the Member States of the UNODC adopted Resolution 23/1, which called for "Strengthening a targeted crime prevention and criminal justice response to combat illicit trafficking in timber and forest products." The

resolution emphasizes the need to develop new tools and technologies to effectively address this criminal enterprise.

Today, illegal timber logging in the Amazon region is widespread, with criminal organizations employing sophisticated technologies to evade law enforcement. These activities result in significant financial losses for the country and exacerbate deforestation, leading to harmful environmental, climatic, and socioeconomic consequences associated with losing native vegetation in such an ecologically sensitive region as the Amazon (Lapola et al., 2023). Therefore, curbing illegal logging is imperative, and enhancing the capacity of law enforcement agencies with better tools is crucial, as pointed out in the above paragraph. Currently, the primary mechanism to combat illegal logging in Brazil is

* Corresponding author.

E-mail address: anaclaudiabatista89@gmail.com (A. Batista).

<https://doi.org/10.1016/j.foreco.2025.122963>

Received 6 February 2025; Received in revised form 26 June 2025; Accepted 28 June 2025

Available online 2 July 2025

0378-1127/© 2025 Elsevier B.V. All rights are reserved, including those for text and data mining, AI training, and similar technologies.

the “Forest Origin Document” (DOF - *Documento de Origem Florestal*), a significant advancement that requires timber producers to provide the geographical coordinates (latitude/longitude) of the logging area, which must be approved following the so-called Sustainable Forest Management Plan (SFMP) (MMA, 2016). However, the plan itself and the DOF are vulnerable to various forms of tampering (Brancalion et al., 2018; Costa et al., 2024; Franca et al., 2023). For example, the document may indicate that the timber originated from a legally authorized area with a permitted logging volume estimated by the SFMP, while the wood may have been harvested from a restricted area where logging is prohibited. This loophole highlights the urgent need for developing surveillance and certification tools to support DOF efforts and prevent illegal exploitation.

Enhancing the surveillance of illegal logging requires developing independent certification tools for provenancing wood to avoid relying exclusively on documentary proof of legality. Wood has geographically specific intrinsic properties including wood anatomy, genetic composition (DNA), and organic and inorganic chemical constituents (Dormontt et al., 2015). One of the most promising tools for proving illegal material is the use of intrinsic chemical markers called stable isotopes, which have been broadly used in material forensics. However, research in this area is still limited to illegal logging, with existing studies showing mixed successes in tracking the provenance of wood (Low et al., 2022). Therefore, further tests and development are necessary to quantify the potential of this method for wood provenance.

Isotope provenance relies on the comparison of a tissue of unknown origin (e.g., a wood sample) with a baseline map called an isoscape predicting the isotope patterns in the tissue of interest across the region of interest (e.g., Amazon forest). Through this comparison, one can produce probabilistic maps of potential origin for the tissue of unknown origin called geographic assignments (Ma et al., 2020). Interestingly, different isotope systems (e.g., strontium, carbon, oxygen) have distinct spatial patterns on the landscape because they depend on different environmental controls (Bataille et al., 2021). As such, they provide independent evidence of the potential origin of a target sample. Consequently, combining multiple isotopes can often provide a way to certify wood provenance precisely or, at the very least, an approach to validate other independent provenance information (e.g., DOF). Several isotopes have shown promise for this provenance purpose, including oxygen, carbon, and strontium isotopes (Gori et al., 2018; Geldern et al., 2006; Watkinson et al., 2020; Mart Vlam et al., 2025).

Strontium has four stable isotopes: ^{84}Sr (~0.56 %), ^{86}Sr (~9.86 %), ^{87}Sr (~7.0 %), ^{88}Sr (~82.58 %). The ratio of $^{87}\text{Sr}/^{86}\text{Sr}$ is frequently used in geological and environmental sciences (Bataille et al., 2020), including in wood provenance (D’Andrea et al., 2023; Hajj et al., 2017; Kafino et al., 2024; Reynolds et al., 2005). This isotope system is particularly useful for the geographic provenance of biological material because the $^{87}\text{Sr}/^{86}\text{Sr}$ ratios in biological substrates vary with the local geology (Bataille and Bowen, 2012). This ratio varies predictably on the landscape due to the constant radioactive decay of ^{87}Rb to ^{87}Sr . As a result, older rocks and/or rocks with more ^{87}Rb (e.g., rocks derived from the continental crust) usually display higher ratios than younger rocks and/or with lower ^{87}Rb (e.g., rocks derived from the mantle) (Bataille and Bowen, 2012). In the last decades, several $^{87}\text{Sr}/^{86}\text{Sr}$ isoscapes were developed in different countries or regions of the world due its usefulness for geographic provenance (Bataille et al., 2020; Evans et al., 2010; Ladegaard-Pedersen et al., 2020; Lugli et al., 2022; Snoeck et al., 2020; Wang et al., 2024; Armaroli et al., 2024).

The Amazon forest has a uniquely varied geology with rock units displaying a huge range of lithology and age with likely large variations in their $^{87}\text{Sr}/^{86}\text{Sr}$ ratios making it an ideal location to apply $^{87}\text{Sr}/^{86}\text{Sr}$ provenance (Bataille et al., 2020). A few hydrological studies have highlighted this potential showing a broad range of $^{87}\text{Sr}/^{86}\text{Sr}$ ratios in rivers and tributaries of the Amazon watershed (Hegg et al., 2015a). For instance, rivers draining younger Cenozoic sediments derived from the Andes, like the Amazon, show lower $^{87}\text{Sr}/^{86}\text{Sr}$ ratios than those draining

older plutonic rocks in the Brazilian and Guiana Shields, such as the Negro and Tapajós rivers (Gaillardet et al., 1997; Santos et al., 2015). The patterns of $^{87}\text{Sr}/^{86}\text{Sr}$ ratios across the Amazon watershed has been used to trace the migration routes of Amazonian catfish (Hegg et al., 2015b). In spite of the potential of this region for using $^{87}\text{Sr}/^{86}\text{Sr}$ provenance, we are not aware of other studies leveraging $^{87}\text{Sr}/^{86}\text{Sr}$ ratios for solving some of the most critical sustainability and biodiversity challenges of the Amazon region.

Although rocks are the main source of Sr to ecosystems, there are several other processes that can alter the propagation of $^{87}\text{Sr}/^{86}\text{Sr}$ ratios from rocks to soils, waters, and organisms, complicating the modeling of $^{87}\text{Sr}/^{86}\text{Sr}$ ratios in plants (Bataille et al., 2020). For instance, the mixing of rock sources by tectonic events and erosion, differential weathering rates of rock units or minerals in soils, and uptake of strontium from different layers of the soil due to distinct root depths between plant species can all lead to divergence between bedrock $^{87}\text{Sr}/^{86}\text{Sr}$ and plant $^{87}\text{Sr}/^{86}\text{Sr}$ ratios. Additionally, atmospheric inputs from sea salt, ashes, and dust may also add some exogenous sources of Sr to ecosystems, further differentiating ecosystems $^{87}\text{Sr}/^{86}\text{Sr}$ from its local bedrock. Therefore, to properly trace the provenance of wood, it is most appropriate to model the $^{87}\text{Sr}/^{86}\text{Sr}$ patterns in the bioavailable strontium pool, which is reflected in the $^{87}\text{Sr}/^{86}\text{Sr}$ of plants and organisms. Bataille et al., (2020) leveraged a large database of $^{87}\text{Sr}/^{86}\text{Sr}$ in plants and a collection of high-resolution geospatial variables representing geology, climate, atmospheric deposition and soil to map bioavailable $^{87}\text{Sr}/^{86}\text{Sr}$ ratios across the globe using a random forest framework. They demonstrated how this approach could accurately map bioavailable $^{87}\text{Sr}/^{86}\text{Sr}$ across the globe with the Amazon region showing large $^{87}\text{Sr}/^{86}\text{Sr}$ variations following the geology. However, the global bioavailable $^{87}\text{Sr}/^{86}\text{Sr}$ isoscape was constructed without any plant or animal samples from the Amazon. It only included a few $^{87}\text{Sr}/^{86}\text{Sr}$ ratios from the Amazon River watershed (Bataille et al., 2020). Bataille et al. (2020) demonstrated that this global isoscape was not accurate for data-poor regions, particularly in areas with old rock units like the Amazon region. Consequently, plant $^{87}\text{Sr}/^{86}\text{Sr}$ data are required to accurately predict the $^{87}\text{Sr}/^{86}\text{Sr}$ in trees from the Amazon.

Our goal is to develop a tree $^{87}\text{Sr}/^{86}\text{Sr}$ isoscape for the Amazon region to allow $^{87}\text{Sr}/^{86}\text{Sr}$ provenance of wood and support law enforcement agencies in combating illegal logging. To that end, we launched an extensive sampling program across the Amazon two years ago. We collected samples from approximately 266 trees across 22 sampling areas throughout the region. From this dataset, we selected 3 individuals in most of the sites from 21 sampling areas, resulting in a total of 67 trees analyzed for $^{87}\text{Sr}/^{86}\text{Sr}$. While this represents a relatively small number of plots given the vast size of the Amazon, this sampling campaign was resource-intensive both in time and cost due to the remoteness of these regions. We constructed $^{87}\text{Sr}/^{86}\text{Sr}$ isoscapes using two different approaches: regression kriging and random forest, which have been previously applied to create accurate bioavailable $^{87}\text{Sr}/^{86}\text{Sr}$ isoscapes in other regions (Bataille et al., 2020; Lugli et al., 2022). Our secondary objective is to assess the predictive potential of these isoscapes and their uncertainties to identify regions where additional sampling is needed. This is particularly important given the high sample collection costs in the Amazon region. While more data are required to produce a high-resolution $^{87}\text{Sr}/^{86}\text{Sr}$ isoscape, our dataset is an initial step towards a comprehensive isoscape of the Amazon region with significant implications for protecting the Amazon Forest from illegal logging and expanding the use of $^{87}\text{Sr}/^{86}\text{Sr}$ provenance to other sustainability, forensics and biodiversity challenges in this critical region.

2. Material and methods

2.1. Wood sampling

In this study, we selected 67 trees from our original dataset for $^{87}\text{Sr}/^{86}\text{Sr}$ analysis across 21 sampling areas in the Brazilian Amazon

region (Fig. 1). These areas were strategically distributed to capture the geological diversity of the region, as illustrated in the geological map of the Brazilian Amazon. Fig. 1 highlights the major lithostratigraphic units, grouped by geochronological categories. The Amazon Basin is bordered by ancient crystalline rocks of the Guiana Shield to the north and the Brazilian Shield to the south, both dominated by Precambrian formations. Between these shields lies the Cenozoic Trough, filled predominantly with younger Cenozoic sediments that characterize the central lowlands. Additionally, transitional zones particularly near the basin margins contain Paleozoic and Mesozoic rocks, including Cretaceous, Jurassic, and Triassic units. Neoproterozoic formations and other unmapped or undifferentiated units are scattered throughout the basin, contributing to the region's complex geolithological framework and influencing the spatial variability in $^{87}\text{Sr}/^{86}\text{Sr}$ signatures.

For some sampling areas, the longitude and latitude of each individual were recorded, while for other sites, only a single coordinate point represents all individuals in this sampling area (Table 1). This discrepancy arises because our dataset includes samples collected by various partners and contributions from collaborators who collected trees for unrelated purposes and did not record individual geographic coordinates. We established a sampling protocol that was followed most of the time but not consistently for the above reasons. We targeted the three most common species for logging, including the genus *Cedrela*, and *Handroanthus*. However, since these genera were not always available, other species were included. Entire wood cross-sections of approximately 3–8 cm in width were collected and extracted from the base of the cross-sections. Sample came from the permanent collection of the Dendrochronology Laboratory at UFLA, and these cross-sections were transported to the Wood Anatomy and Identification Laboratory of the Escola Superior de Agricultura “Luiz de Queiroz” where they were polished until any eventual ring structure became visible. Radial strips were sawed from the cross-sections with a band saw. From the radial strips, we saw five 2-cm-long pieces: one at the center of the cross-sections and four others at equal intervals corresponding to 25 %, 50 %, 75 %, and 100 % (bark) from the total length between the disk center to the outermost bark. The 2-cm-long pieces for most of the samples encompassed 5–7 rings.

Although ideally all specimens would have been analyzed, the high

cost of strontium analysis — exacerbated by the unfavorable exchange rate between the Brazilian Real and the US Dollar — limited us to selecting only three specimens per sampling site. Whenever possible, we selected specimens from the same genus or species at each site; however, this was not always feasible. As a result, some sites contain specimens from different genera (Table 1). For each sample, we selected a sample from the same area of the tree disk, a 2-cm-long piece from the radial strips (75 %), which generally correspond to the end of the heartwood. We analyzed a total of 67 wood samples.

2.2. Strontium analyses

Strontium isotope analyses were conducted in the Radiogenic Isotope and Geochronology Laboratory (RIGL) at Washington State University, Pullman, USA. All samples (approximately 100 mg each) for $^{87}\text{Sr}/^{86}\text{Sr}$ analysis were digested in 7 mL Savillex™ branded PFA vials using a mixture of 1 mL of 50 % Hydrogen Peroxide (reagent grade) and 2 mL of concentrated double distilled nitric acid (HNO_3) for 1 h at room temperature (approximately 20 °C). After initial dissolution, the solutions were dried on a hot plate at 60 °C on a cross flow ventilated hot-plate. Once dry each sample was re-treated with the same acid mixture as above to ensure complete reaction and then taken back to dryness at 60 °C. The dissolved Sr sample was twice processed through a micro-column loaded with Sr-spec Resin™ (100–150 µm; Eichrom Technologies, LLC). The samples were dissolved with 0.4 mL of 8 M HNO_3 , centrifuged at 3500 rpm for 15 min, and loaded onto the microcolumns. The matrix was rinsed using 3 M HNO_3 . The Sr was collected with 0.5 M HNO_3 . After separation, the eluted solutions were dried and re-dissolved in 1 mL of 2 % v/v HNO_3 for $^{87}\text{Sr}/^{86}\text{Sr}$ analysis. The $^{87}\text{Sr}/^{86}\text{Sr}$ analysis was performed at 200 ppb concentration using a Thermo Scientific Neptune Plus multi-collector inductively coupled plasma mass spectrometer (MC-ICP-MS). The solution was aspirated using a PFA nebulizer, a double-pass quartz spray chamber, quartz torch, and nickel sample and skimmer cones. Isotopes ^{82}Kr , ^{83}Kr , ^{84}Sr , ^{85}Rb , ^{86}Sr , ^{87}Sr , and ^{88}Sr were simultaneously measured in L4, L3, L2, L1, C, H1, and H2 Faraday cups, respectively. Measurements of samples were made using a static multi-collector routine that consisted of 1 block of 60 cycles with an integration time of 8 s/cycle. ^{84}Sr , ^{86}Sr and ^{87}Sr were in run corrected

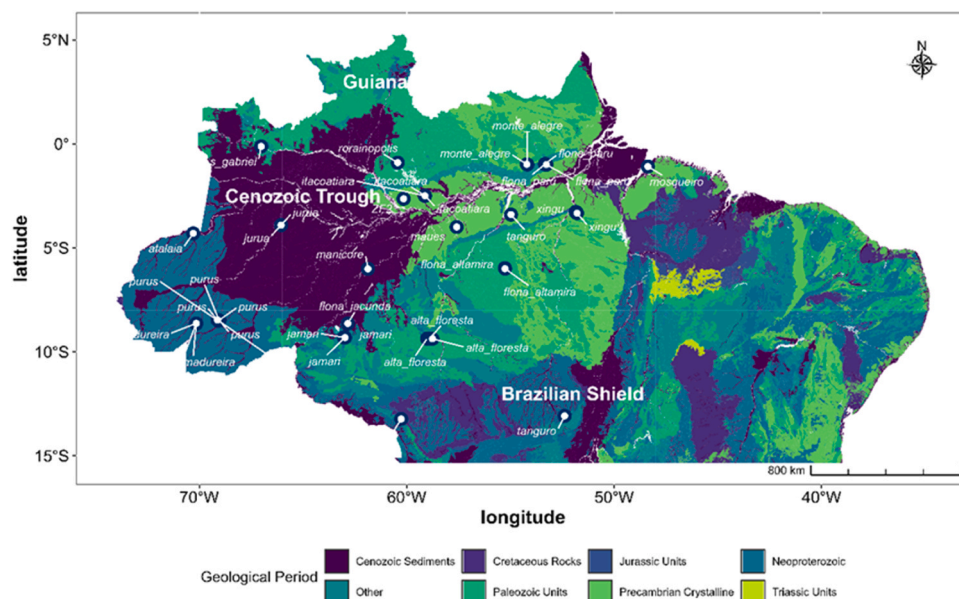


Fig. 1. Geological map of the Brazilian Amazon showing the distribution of lithological units by geological period, major geomorphological features, and sampling locations. Colored areas represent distinct geological units grouped by minimum formation age: Cenozoic Sediments, Cretaceous Rocks, Jurassic Units, Triassic Units, Paleozoic Units, Neoproterozoic, Precambrian Crystalline, and Other. Major geomorphological features are annotated, including the Guiana Shield, Brazilian Shield, and the Cenozoic Trough. White circles indicate sampling sites.

Table 1

The $^{87}\text{Sr}/^{86}\text{Sr}$ ratios of 67 tree wood collected from various areas in the Brazilian Amazon (Fig. 1), along with their geographical coordinates, botanical genus and family, and the underlying geologic features. The Brazilian and Guiana Shields are predominantly composed of Precambrian rocks, while Cenozoic deposits primarily characterize the intervening areas.

Lab.code	Longitude	Latitude	Area	Genus	Family	$^{87}\text{Sr}/^{86}\text{Sr}$	Geologic feature
mad623	-59.0190	-9.3650	alta_floresta	Goupeia	Euphorbiaceae	0.795554	Brazilian_shield
mad628	-58.8900	-9.3550	alta_floresta	Manilkara	Sapotaceae	0.762186	Brazilian_shield
mad630	-58.7600	-9.3710	alta_floresta	Manilkara	Sapotaceae	0.773279	Brazilian_shield
mad21	-70.2911	-4.3037	atalaia	Iryanthera	Myristicaceae	0.714738	Cenozoic_deposits
mad28	-70.2911	-4.3037	atalaia	Iryanthera	Myristicaceae	0.717219	Cenozoic_deposits
mad13	-70.2911	-4.3037	atalaia	Protium	Burseraceae	0.713565	Cenozoic_deposits
mad732	-55.2700	-5.9700	flona_altamira	Cedrela	Meliaceae	0.762904	Brazilian_shield
mad728	-55.2700	-5.9700	flona_altamira	Cedrela	Meliaceae	0.762949	Brazilian_shield
mad726	-55.2600	-6.0000	flona_altamira	Cedrela	Meliaceae	0.7457	Brazilian_shield
mad722	-62.8390	-8.6360	flona_jacunda	Manilkara	Sapotaceae	0.759167	Brazilian_shield
mad769	-53.3300	-0.9800	flona_paru	Cedrela	Meliaceae	0.722397	Cenozoic_deposits
mad765	-53.3300	-0.9600	flona_paru	Cedrela	Meliaceae	0.723057	Cenozoic_deposits
mad766	-53.2700	-1.0000	flona_paru	Cedrela	Meliaceae	0.727752	Cenozoic_deposits
mad73	-59.1260	-2.4860	itacoatiara	Mezilaurus	Lauraceae	0.726116	Cenozoic_deposits
mad71	-59.1190	-2.4950	itacoatiara	Mezilaurus	Lauraceae	0.724649	Cenozoic_deposits
mad72	-59.1190	-2.4940	itacoatiara	Mezilaurus	Lauraceae	0.724447	Cenozoic_deposits
mad651	-63.0310	-9.3040	jamari	Cedrelinga	Fabaceae	0.744177	Brazilian_shield
mad650	-62.9800	-9.3150	jamari	Cedrelinga	Fabaceae	0.75052	Brazilian_shield
mad649	-62.9740	-9.3130	jamari	Cedrelinga	Fabaceae	0.757047	Brazilian_shield
mad34	-66.0551	-3.9072	jurua	Iryanthera	Myristicaceae	0.725331	Cenozoic_deposits
mad40	-66.0551	-3.9072	jurua	Iryanthera	Myristicaceae	0.728354	Cenozoic_deposits
mad24	-66.0550	-3.9070	jurua	Iryanthera	Myristicaceae	0.729134	Cenozoic_deposits
mad20	-61.8687	-6.0097	manicore	Iryanthera	Myristicaceae	0.741098	Cenozoic_deposits
mad35	-61.8687	-6.0097	manicore	Iryanthera	Myristicaceae	0.741573	Cenozoic_deposits
mad19	-61.8687	-6.0097	manicore	Iryanthera	Myristicaceae	0.738389	Cenozoic_deposits
mad1	-57.5893	-3.9955	maues	Protium	Burseraceae	0.728269	Cenozoic_deposits
mad26	-57.5893	-3.9955	maues	Protium	Burseraceae	0.740075	Cenozoic_deposits
mad5	-57.5893	-3.9955	maues	Protium	Burseraceae	0.727018	Cenozoic_deposits
mad739	-54.1800	-0.9900	monte_alegre	Cedrela	Meliaceae	0.723396	Cenozoic_deposits
mad744	-54.2100	-0.9800	monte_alegre	Cedrela	Meliaceae	0.714456	Cenozoic_deposits
mad745	-54.1800	-0.9900	monte_alegre	Cedrela	Meliaceae	0.720443	Cenozoic_deposits
mad617	-48.3732	-1.0888	mosqueiro	Dipteryx	Fabaceae	0.712152	Cenozoic_deposits
mad618	-48.3732	-1.0888	mosqueiro	Swartzia	Fabaceae	0.710973	Cenozoic_deposits
mad753	-69.1000	-8.4900	purus	Cedrela	Meliaceae	0.71285	Cenozoic_deposits
mad747	-69.0700	-8.5000	purus	Cedrela	Meliaceae	0.71186	Cenozoic_deposits
mad750	-69.0300	-8.4900	purus	Cedrela	Meliaceae	0.713004	Cenozoic_deposits
mad751	-69.0600	-8.4900	purus	Cedrela	Meliaceae	0.710959	Cenozoic_deposits
mad752	-69.0500	-8.4800	purus	Cedrela	Meliaceae	0.711271	Cenozoic_deposits
mad749	-69.1200	-8.4700	purus	Cedrela	Meliaceae	0.711955	Cenozoic_deposits
mad502	-60.4341	-0.9036	rorainopolis	Dinizia	Fabaceae	0.734653	Guiana_shield
mad503	-60.4341	-0.9036	rorainopolis	Dinizia	Fabaceae	0.79109	Guiana_shield
mad500	-60.4341	-0.9036	rorainopolis	Goupeia	Euphorbiaceae	0.768181	Guiana_shield
mad499	-60.4341	-0.9036	rorainopolis	Manilkara	Sapotaceae	0.817202	Guiana_shield
mad505	-60.4341	-0.9036	rorainopolis	Manilkara	Sapotaceae	0.810259	Guiana_shield
mad499	-60.4341	-0.9036	rorainopolis	Manilkara	Sapotaceae	0.817138	Guiana_shield
mad505	-60.4341	-0.9036	rorainopolis	Manilkara	Sapotaceae	0.810276	Guiana_shield
mad10	-67.0131	-0.1212	s_gabriel	Protium	Burseraceae	0.769935	Guiana_shield
mad25	-67.0131	-0.1212	s_gabriel	Protium	Burseraceae	0.720606	Guiana_shield
mad31	-67.0131	-0.1212	s_gabriel	Protium	Burseraceae	0.764545	Guiana_shield
mad683	-70.1580	-8.6490	sena_madureira	Handroanthus	Bignoniaceae	0.711105	Cenozoic_deposits
mad667	-70.1500	-8.6500	sena_madureira	Handroanthus	Bignoniaceae	0.711207	Cenozoic_deposits
mad666	-70.1450	-8.6320	sena_madureira	Handroanthus	Bignoniaceae	0.711632	Cenozoic_deposits
mad89	-54.9740	-3.3984	tanguro	Hymenaea	Fabaceae	0.726185	Brazilian_shield
mad591	-52.3864	-13.0790	tanguro	Nectandra	Fabaceae	0.726483	Brazilian_shield
mad590	-52.3864	-13.0790	tanguro	Tratinnickia	Burseraceae	0.72616	Brazilian_shield
mad84	-54.9740	-3.3984	tapajos	Hymenaea	Fabaceae	0.727044	Cenozoic_deposits
mad85	-54.9740	-3.3984	tapajos	Hymenaea	Fabaceae	0.725546	Cenozoic_deposits
mad83	-54.9740	-3.3984	tapajos	Manilkara	Sapotaceae	0.726068	Cenozoic_deposits
mad571	-60.2674	-13.2300	vilhena	Bowdichia	Fabaceae	0.737892	Brazilian_shield
mad567	-60.2674	-13.2300	vilhena	Nectandra	Lauraceae	0.726238	Brazilian_shield
mad567	-60.2674	-13.2300	vilhena	Nectandra	Lauraceae	0.737751	Brazilian_shield
mad756	-51.8500	-3.2700	xingu	Bertholletia	Lecythidaceae	0.734375	Brazilian_shield
mad754	-51.8500	-3.2700	xingu	Cedrela	Meliaceae	0.730093	Brazilian_shield
mad762	-51.7900	-3.3300	xingu	Cedrela	Meliaceae	0.727563	Brazilian_shield
mad48	-60.1497	-2.6380	ZF2	Anacardium	Anacardiaceae	0.721791	Cenozoic_deposits
mad44	-60.1497	-2.6380	ZF2	Brosimum	Moraceae	0.723224	Cenozoic_deposits
mad49	-60.1497	-2.6380	ZF2	Scleronema	Malvaceae	0.723249	Cenozoic_deposits

for ^{84}Kr , ^{86}Kr , ^{87}Rb isobaric interferences. Instrumental mass fractionation was corrected by normalizing $^{86}\text{Sr}/^{88}\text{Sr}$ to 0.1194 using the exponential law. Strontium isotope compositions are reported as $^{87}\text{Sr}/^{86}\text{Sr}$ ratios. The RIGL 2023–2024 reproducibility of the $^{87}\text{Sr}/^{86}\text{Sr}$ measurement of NIST SRM987 from January 17, 2023, to December 11, 2024, is 0.710275 ± 23 (2 SD, $n = 256$).

2.3. Descriptive statistics

We present descriptive statistics for the 67 trees and an analysis of variance to determine which covariates are the main drivers of $^{87}\text{Sr}/^{86}\text{Sr}$ variance. This analysis included the sampling site, genus, and geological provinces as random variables in a generalized linear model (GLM). To test the differences of $^{87}\text{Sr}/^{86}\text{Sr}$ ratio of tree woods grouped according to geological provinces, we also used a GLM, but in this run, geological provinces were a fixed predictor, and sampling sites and genus were random variables, with genus nested on sampling sites. We also explore the within-site variability by graphically comparing the $^{87}\text{Sr}/^{86}\text{Sr}$ ratio between specimens of the same sampling area.

2.4. Regression kriging

We chose not to use the $^{87}\text{Sr}/^{86}\text{Sr}$ ratios from all 67 trees for the kriging interpolation. Instead, for sampling areas without individual tree coordinates, we averaged the $^{87}\text{Sr}/^{86}\text{Sr}$ ratios of all trees in the area and assigned the average to the area's geographic coordinates. We retained the data for each tree for sampling areas with individual tree coordinates. This approach resulted in 40 data points with coordinates (Table 1). Aggregating data is justified because kriging assumes independent spatial observations, an assumption violated when multiple values share the same location (Goovaerts, 1997). Additionally, assigning identical coordinates to multiple trees creates artificial clustering, which can distort the variogram and kriging predictions.

We used regression kriging (Willmes et al., 2018) as a starting approach to map $^{87}\text{Sr}/^{86}\text{Sr}$ patterns based on the good performance of this approach to map soil geochemistry (Hengl et al., 2007). This method combines the spatial interpolation of observations with regression-based interpolation using spatially distributed auxiliary variables. We tested a couple of potential auxiliary variables to map $^{87}\text{Sr}/^{86}\text{Sr}$ ratios including rock age and the previously generated global bioavailable $^{87}\text{Sr}/^{86}\text{Sr}$ isoscape by Bataille et al. (2020). Both models produced similar results. However, the residuals of the model using bioavailable $^{87}\text{Sr}/^{86}\text{Sr}$ followed a normal distribution (Shapiro-Wilk test: $W = 0.98$, $p = 0.60$), whereas the residuals of the model using rock age did not meet the normality assumption ($W = 0.93$, $p = 0.02$). Since kriging assumes that the residuals follow a normal distribution to ensure unbiased predictions and accurate uncertainty estimates, we selected bioavailable $^{87}\text{Sr}/^{86}\text{Sr}$ as the covariate for regression kriging.

The regression-kriging analysis was performed using the *automap* package in R (Hiemstra et al., 2009). This package has one advantage over others that perform kriging analysis: *automap* automatically selects the best semivariogram model to be used in the kriging interpolation itself. To minimize the influence of outliers in our kriging model, we used a robust semivariogram estimation method by setting *creessie* = TRUE. This approach, based on the Cressie-Hawkins robust estimator, reduces the sensitivity of the semivariogram calculation to extreme values in the data (Cressie and Hawkins, 1980). By focusing on the median and more stable aspects of the data's spatial structure, the robust semivariogram provides a more reliable representation of spatial variability, ensuring that the kriging model is less biased by outlier effects.

The quality of the spatial predictions and the comparison of the kriging models were evaluated using diagnostic measures, mean absolute error (MAE), and root mean square error (RMSE) estimated by 10-fold cross-validation using the *autoKrige.cv()* of the *automap* package. Finally, we estimated coefficient of determination (R^2) by comparing the observed $^{87}\text{Sr}/^{86}\text{Sr}$ ratios with those predicted by the cross-validation.

We also used the *automap* package (via kriging) to generate a spatially explicit map of uncertainty (i.e., standard deviation). This map, along with the mean prediction, is required for generating proper Bayesian geographic assignments required for provenance wood (Ma et al., 2020).

2.5. Random forest

For consistency, we used the same 40 data points in the Random Forest and kriging models (Table S1). We developed a wood $^{87}\text{Sr}/^{86}\text{Sr}$ isoscape using random forest regression, following an approach similar to that of Bataille et al. (2020). We tested several potential climatic, topographic, and geological variables (Table S2). However, we did not include the variable bioavailable $^{87}\text{Sr}/^{86}\text{Sr}$ ratio estimated by Bataille et al. (2020) because it was derived using covariates similar to those used in our Random Forest model, which could lead to overfitting. We used the R package *VSURF* for variable selection (Genuer et al., 2015). We chose to work with the variables selected by the 'threshold' mode of the *VSURF* library because this mode focuses on the initial screening of variables based on their importance scores, removing those with minimal contribution to the response variable. The selection process at the threshold level of the *VSURF* identified all covariates listed in Table S2 as important to the model. Using these predictors, we trained a Random Forest model with wood $^{87}\text{Sr}/^{86}\text{Sr}$ ratios as the dependent variable. The model was configured with 10,000 trees, and we used a 10-fold cross-validation to optimize the training process. Model performance was checked by computing the coefficient of determination (R^2), the root means square error (RMSE), and the mean absolute error (MAE) on the cross-validation results. Likewise, we estimated R^2 by comparing the observed $^{87}\text{Sr}/^{86}\text{Sr}$ ratios with those predicted by the cross-validation.

We then applied the model spatially using the continuous covariates selected by *VSURF*, to map $^{87}\text{Sr}/^{86}\text{Sr}$ ratios across the study area. Spatial estimates of uncertainty are not provided in the random forest regression. We computed an uncertainty map using Quantile Random Forest implemented with the *ranger* and *caret* R packages (Kuhn, 2008; Wright and Ziegler, 2017), following the script available at [https://doi.org/10.5281/zenodo.14801392]. To estimate the standard deviation for constructing the uncertainty map and comparing it with the one generated by the Kriging model, we first created rasters for the 0.5 and 0.841 quantiles. The standard deviation was approximated by subtracting the 0.5 quantile raster from the 0.841 quantile raster, under the assumption of a normal distribution of residuals.

Using the random forest model, we estimated the relative importance of each predictive variable with the *party* R package, which implements a conditional inference framework for unbiased recursive partitioning (Hothorn et al., 2006). This method provides a more interpretable measure of importance, reflecting the variable's direct contribution to model accuracy. Using only the most important covariates, we generated partial dependence plots (PDPs) to examine the relationships between key predictive variables and $^{87}\text{Sr}/^{86}\text{Sr}$ ratios, using the *pdp* R package (Greenwell, 2017).

2.6. Comparison of isoscapes

We compared spatial differences between isoscapes produced by Kriging and Random Forest approaches by estimating the difference between their predictions on a grid containing 135,505 pairs of longitude and latitude points. This difference was then normalized by dividing it by the range of $^{87}\text{Sr}/^{86}\text{Sr}$ ratios across the entire dataset (0.1017) and multiplying by 100, resulting in a relative difference expressed as a percentage of the range. To handle both negative and positive differences, we used absolute values. Based on the histogram of those absolute differences, we categorized them into three groups: low (<12 %), medium (12–22 %), and high (>22 %) to produce a map of similarity between models.

3. Results

3.1. Range of $^{87}\text{Sr}/^{86}\text{Sr}$ ratios in trees across the Amazon forest

The average $^{87}\text{Sr}/^{86}\text{Sr}$ ratio and 95 % confidence interval among 67 tree samples were 0.73757 (0.73094, 0.74421). The Sr ratios ranged from a minimum of 0.71096 to a maximum of 0.81720 across the 67 samples, yielding a total range of 0.10624 (Table 2). Fig. 2 presents the $^{87}\text{Sr}/^{86}\text{Sr}$ of individual specimens from each sampling area in ascending order. We also grouped trees according to the underlying geological provinces: the younger Cenozoic Amazon Trough (Cenozoic deposits) and the older Brazilian and Guiana Shields to the south and north, respectively. The GLM having geological provinces as a fixed factor and sampling sites and genera as random factors indicated that differences in $^{87}\text{Sr}/^{86}\text{Sr}$ ratios between geological provinces are significant, with the increasing order: Cenozoic Trough<Brazilian Shield<Guiana Shield (Table 2). In the second run of the GLM, we only included random variables (geological provinces, sampling sites and genera) in performing a variance partitioning, in this case, the model explained 83 % of the $^{87}\text{Sr}/^{86}\text{Sr}$ ratio variance, with a significant contribution of geological provinces (63 %), followed by sampling sites (13 %) and genera with only (7 %). Accordingly, the residual was 17 % (Table 2).

3.2. $^{87}\text{Sr}/^{86}\text{Sr}$ local variability

The local variability was generally low, as indicated by the low coefficients of variation, most of which were below 1 % (Table S1). However, three sites, Alta Floresta, Rorainópolis, and São Gabriel da Cachoeira, exhibited higher variability (Fig. 2, Table S1). In Alta Floresta (CV = 2.2 %), located in the southwest part of the Amazon (Fig. 1), on the Brazilian Shield, two specimens of *Manilkara* had the lowest $^{87}\text{Sr}/^{86}\text{Sr}$ ratios (0.7622, 0.7733), which are higher than the overall average ratio (0.7376), and the highest ratio was found for a *Goupeia* tree (0.7954). In this site, each specimen's exact longitude and latitude are available. Each tree is approximately 15 km from each other in the East–West direction.

The highest variability was observed in the Rorainópolis (CV = 3.9 %, Table S1), based on the analysis of seven specimens were analyzed (Fig. 2). Rorainópolis is in the Guiana Shield, northern part of the Amazon (Fig. 1). In this site, four specimens of *Manilkara* had the highest $^{87}\text{Sr}/^{86}\text{Sr}$ ratios among the whole data set (average 0.8137 [0.8098, 0.81762]). There are two specimens of *Dinizia*, which the following ratios of 0.7347 and 0.7911, and one specimen of *Goupeia* with a ratio of 0.7682. Finally, São Gabriel da Cachoeira (CV = 3.6 %, Table S1) is also to the North on the Guiana Shield (Fig. 1). There are three specimens of *Protium*, one with a low $^{87}\text{Sr}/^{86}\text{Sr}$ ratio (0.720606) and the other two with higher and similar $^{87}\text{Sr}/^{86}\text{Sr}$ ratios (0.764545 and 0.769935) (Fig. 2). Unfortunately, Rorainópolis and São Gabriel da Cachoeira were some of the sites where individual specimens lacked geographical coordinates. As a result, we were unable to evaluate the distances between specimens as we did in Alta Floresta.

3.3. Regression kriging

The *automap* package identified a variogram (Sph) model with the

Table 2
Average $^{87}\text{Sr}/^{86}\text{Sr}$ ratios of tree wood (avg), with 95 % confidence intervals and sample counts (count), categorized by the main geological provinces of the Amazon basin.

Provinces	$^{87}\text{Sr}/^{86}\text{Sr}$		count
	avg	95 %CI	
Cenozoic Trough	0.72177	(0.71891, 0.72464)	38
Brazilian Shield	0.74664	(0.73793, 0.75536)	19
Guiana Shiled	0.78039	(0.75894, 0.80184)	10

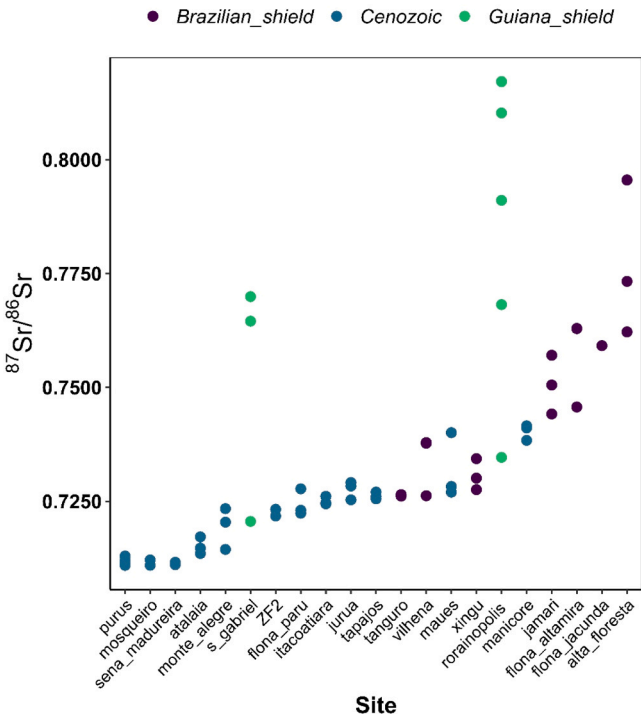


Fig. 2. $^{87}\text{Sr}/^{86}\text{Sr}$ ratios of wood samples, ordered in ascending values, from sampling plots across the Amazon region. The color of the points refers to the underlying geological features.

following parameters: nugget = 1.34×10^{-5} , psill = 1.94×10^{-4} , range = 2.18 degrees (Figure S1). The nugget represents small-scale variability or measurement error, the psill (partial sill) corresponds to the variance explained by spatial autocorrelation, and the range is the distance over which points are spatially correlated. The range is expressed in degrees of longitude/latitude. Given that near the Equator—where the Amazon is located—1 degree corresponds to approximately 111 km, a range of 2.2 degrees translates to about 250 km, indicating a broad scale spatial autocorrelation in this dataset or it is also a reflection of our sampling spatial distribution, since the model could not find a shorter spatial autocorrelation because we have not too many points within the 50–250 km distance. A spatial autocorrelation range of 250 km reflects the broad spatial variability influenced by large-scale geological features (e.g., the Cenozoic Trough, Brazilian Shield, and Guiana Shield). This range appears to have been well captured by the Kriging model, as evidenced by the resemblance between the Kriging isoscape (Fig. 3) and the minimum geological age of the main Amazon geological formations (Fig. 1).

On the other hand, the standard deviation isoscape highlights some concerns about the model's performance (Fig. 4). Two key points stand out. First, the very low standard deviation values and their uniformity across the landscape, coupled with the presence of "bull's-eye" patterns around sampling areas (Fig. 6). These patterns suggest an insufficient number of sampling points across the region, causing the kriging component to rely heavily on local observations (Willmes et al., 2018). Additionally, the variogram used for kriging may not be well-fitted or may fail to capture the spatial structure of the data accurately. This is further evidenced by the semivariogram, which exhibited a few outliers and considerable variability in variance beyond the range (Figure S1). Interestingly, despite these limitations, the regression-kriging model demonstrated moderate to good predictive, with a MAE of 0.00698 (which is equivalent to only 7 % of the $^{87}\text{Sr}/^{86}\text{Sr}$ range), RMSE of 0.01057 (10 % of the range), and R^2 of 0.77.

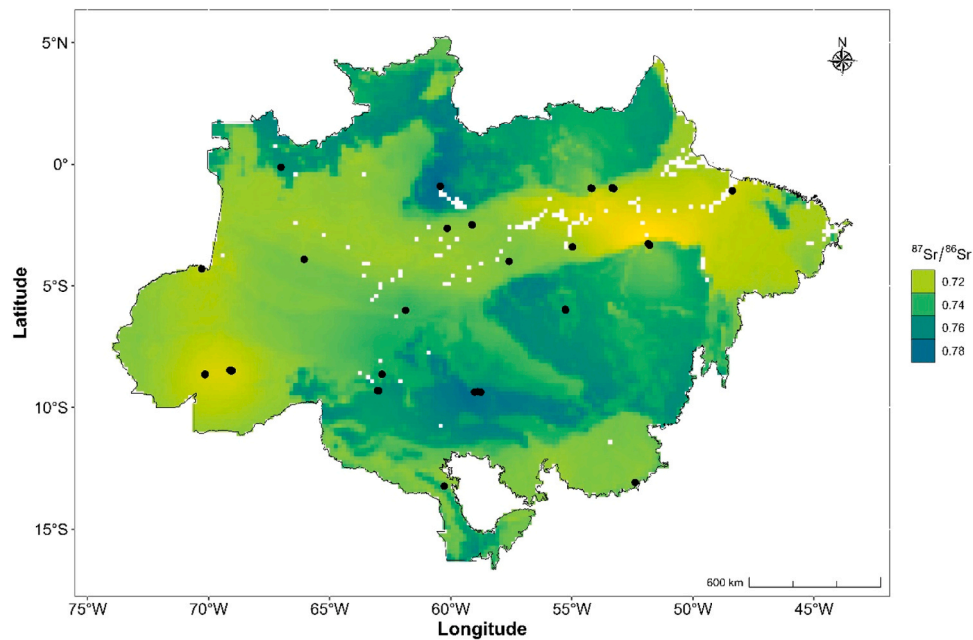


Fig. 3. Isoscape of $^{87}\text{Sr}/^{86}\text{Sr}$ ratios in tree wood, derived through regression kriging. The isoscape uses the bioavailable $^{87}\text{Sr}/^{86}\text{Sr}$ from Bataille et al. (2020) as a predictor variable. Please note the resemblance between this isoscape and the rock age distribution shown in Fig. 1, highlighting the relationship between geological provenance and isotopic composition.

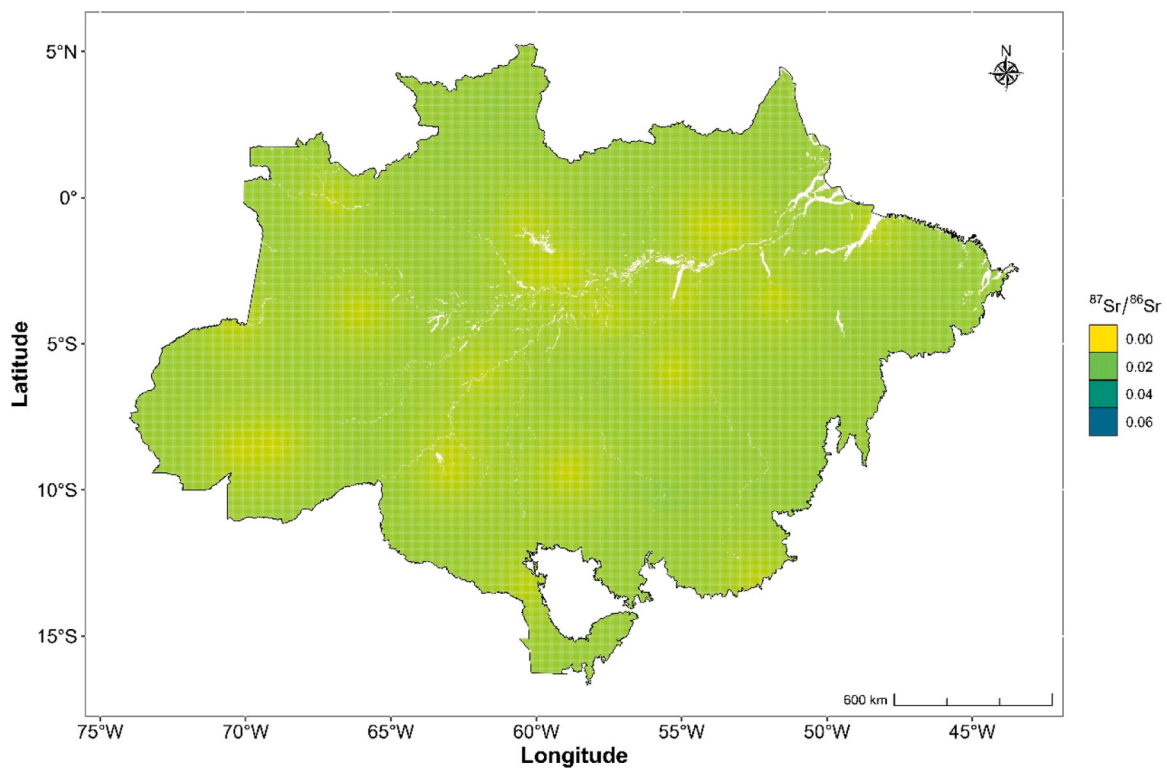


Fig. 4. Isoscape of $^{87}\text{Sr}/^{86}\text{Sr}$ standard-deviations in tree wood, derived through regression kriging. The isoscape uses the bioavailable $^{87}\text{Sr}/^{86}\text{Sr}$ from Bataille et al. (2020) as a predictor variable.

3.4. Random forest

The spatial trends observed in the Random Forest isoscape closely resembled those in the regression kriging approaches (Fig. 5). Areas in the Amazon with older rock formations, such as the Brazilian and Guiana Shields, showed higher $^{87}\text{Sr}/^{86}\text{Sr}$ ratios than younger regions

formed by Cenozoic sediments (Fig. 5). The standard deviation isoscape showed higher standard deviations compared to the isoscape generated by the Kriging model. The range of standard deviations (~ 0.01 to ~ 0.06) indicates that the model predicts relatively low uncertainties across much of the region, with a few notable outliers. Additionally, it avoids the characteristic 'bullseye' patterns often seen near sampling

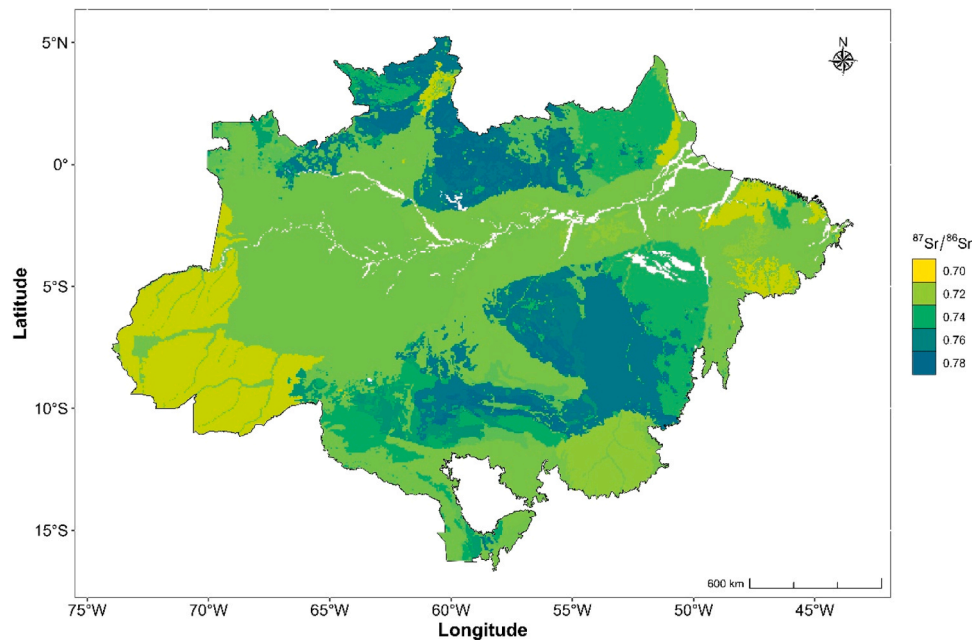


Fig. 5. Isoscape of $^{87}\text{Sr}/^{86}\text{Sr}$ ratios in tree wood, derived through Random Forest. The isoscape uses the average geological age of formations and the vapor atmospheric pressure (VPD) and air relative humidity (RH) as predictor variables. Please note the resemblance between this isoscape and the rock age distribution shown in Fig. 1, highlighting the relationship between geological provenance and isotopic composition.

areas and highlights higher standard deviations in the Shields compared to the Cenozoic sedimentary plains of the Central Amazon (Fig. 6). The MAE, RMSE, and R^2 estimated by cross-validation for the Random Forest model showed a reasonable predictive power, 0.00974 (10 % of the range), 0.01319 (12 % of the range), and 0.62, respectively.

The most important predictor based on the permutation-based method was the minimum age of the rock substrate, with important scores of 0.80. Such importance, together with the GLM (Table S3),

reinforces the importance of rock age in predicting the bioavailable $^{87}\text{Sr}/^{86}\text{Sr}$ ratio (Bataille et al., 2020). Other predictors, including relative humidity (RH) and vapor pressure deficit (VPD), were also selected by VSURF but displayed more limited importance.

The partial dependence plots (PDPs) illustrate the effects of rock age, vapor pressure deficit (VPD), and relative humidity (RH) on the $^{87}\text{Sr}/^{86}\text{Sr}$ ratio in wood, revealing distinct trends. The $^{87}\text{Sr}/^{86}\text{Sr}$ ratio remains relatively constant for rock age in areas with young rocks

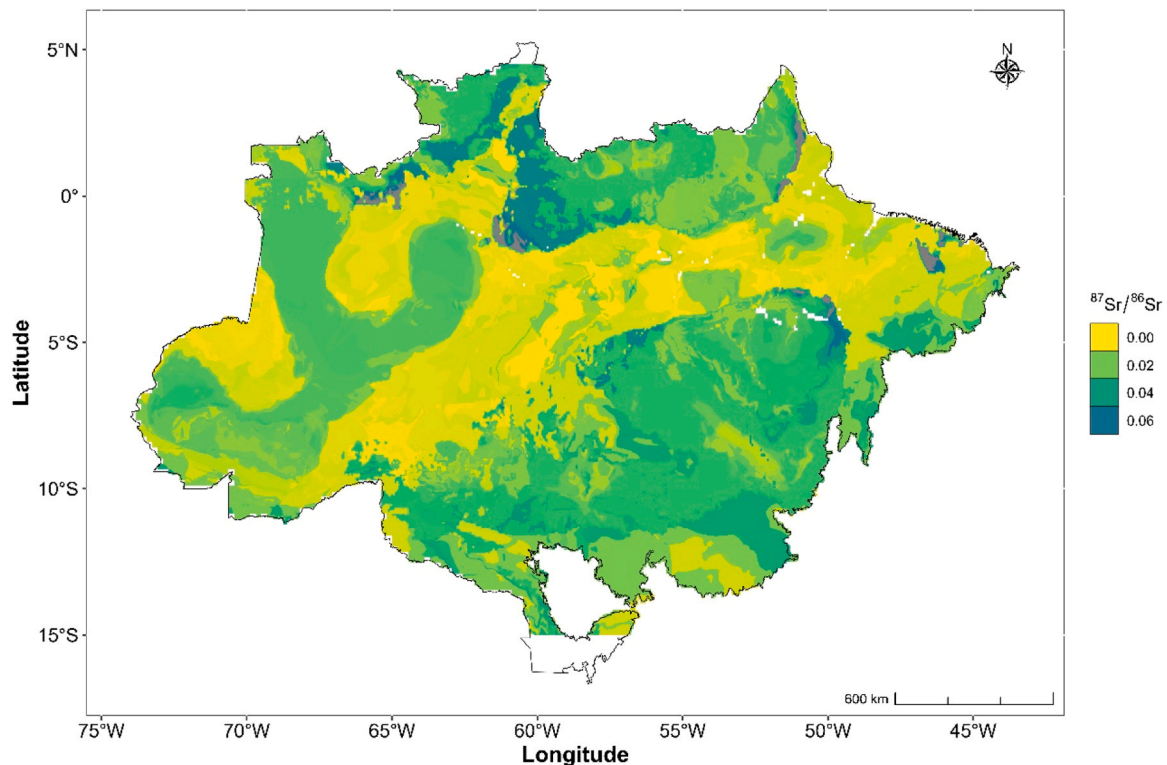


Fig. 6. Isoscape of $^{87}\text{Sr}/^{86}\text{Sr}$ standard-deviations in tree wood, derived through quantile Random Forest.

(<1000 Ma). It shows a slight increase between 1000 and 1500 Ma, followed by a sharp rise in regions with rocks older than 1500 Ma (Fig. 7). In contrast, the PDP for VPD displays a different pattern. Between 0.6 and 0.8 kPa, the $^{87}\text{Sr}/^{86}\text{Sr}$ ratio remains low and constant, followed by an abrupt increase at approximately 0.8 kPa. The ratio then stabilizes at higher values from 0.8 to 1.0 kPa (Fig. 7). Finally, as expected due to its inverse correlation with VPD, the PDP for RH shows an opposite trend. From 0.70–0.75, the $^{87}\text{Sr}/^{86}\text{Sr}$ ratios are relatively high, decreasing sharply between 0.75 and 0.85. Beyond 0.85, the ratios remain constant (Fig. 7).

The combined effect of rock age and VPD on the $^{87}\text{Sr}/^{86}\text{Sr}$ ratios in Amazonian woods is illustrated in the heat map (Fig. 8). Four distinct

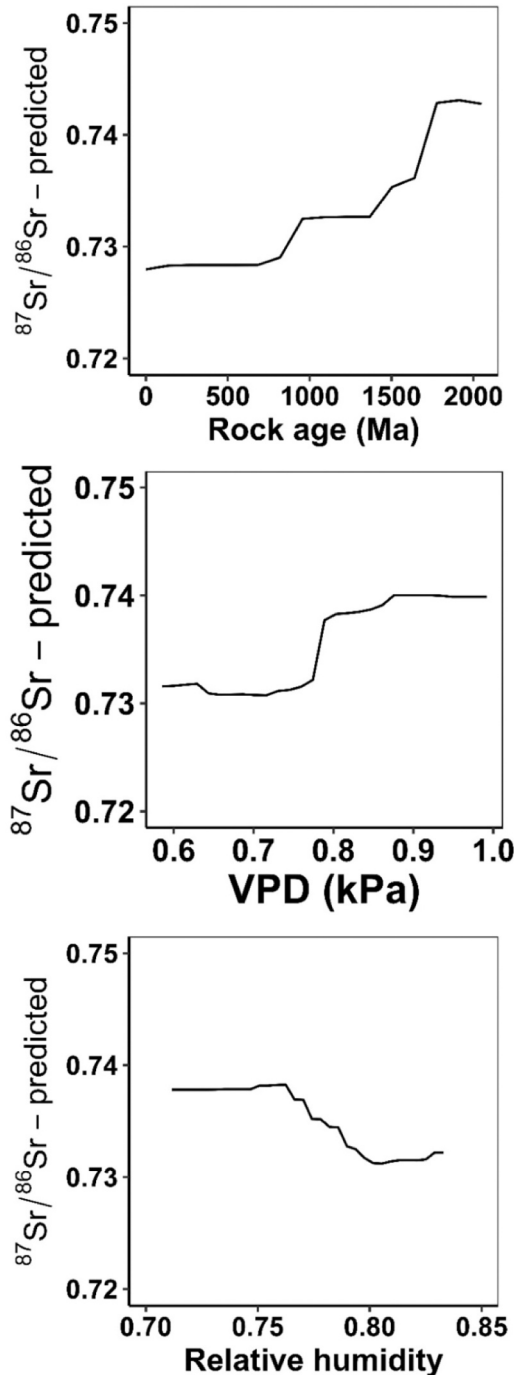


Fig. 7. Partial dependence plots of tree wood $^{87}\text{Sr}/^{86}\text{Sr}$ ratios and minimum rock age, atmospheric vapor pressure deficit, and air relative humidity.

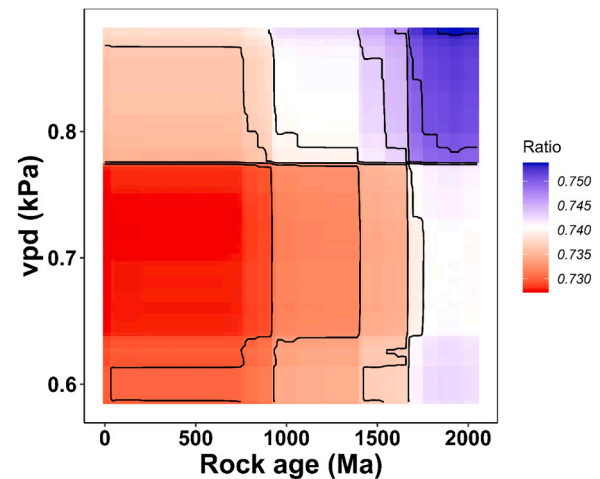


Fig. 8. Interplay between atmospheric vapor deficit (VPD) and geological age in determining bioavailable $^{87}\text{Sr}/^{86}\text{Sr}$ ratios in the wood of the Brazilian Amazon.

quadrants can be observed. The lowest $^{87}\text{Sr}/^{86}\text{Sr}$ ratios are found in regions characterized by younger rocks (<1500 Ma) and wetter (VPD <0.8 kPa). In contrast, the highest $^{87}\text{Sr}/^{86}\text{Sr}$ ratios are associated with regions under older rocks (>1500 Ma) and drier (VPD >0.8 kPa), corresponding to areas with lower relative humidity. Intermediate $^{87}\text{Sr}/^{86}\text{Sr}$ ratios are observed in regions where either younger rock (<1500 Ma) coincide with drier places (VPD > 0.8 kPa) or older rocks (>1500 Ma) occur in wetter places (VPD < 0.8 kPa) (Fig. 8). The heat map between rock age and RH showed an inverse trend (Figure S2).

As detailed in the Material and Methods, we assessed spatial differences between the two isoscapes by plotting the differences as a percentage of the $^{87}\text{Sr}/^{86}\text{Sr}$ range, categorizing these differences as low (<12 %), medium (12–22 %), and high (>22 %). The main differences were found in areas dominated by older rocks, where the variability in $^{87}\text{Sr}/^{86}\text{Sr}$ ratios tend to be higher than in younger rocks (Fig. 9). Approximately 75 % of the map area fell into the “low” difference category, 23 % into “medium,” and only 2 % into the “high” category.

4. Discussion

4.1. Range of $^{87}\text{Sr}/^{86}\text{Sr}$ ratios in the Amazon Forest

The observed variations in bioavailable $^{87}\text{Sr}/^{86}\text{Sr}$ ratios across the Amazon Forest are unparalleled on a global scale. Typically, bioavailable strontium isotopes in terrestrial ecosystems vary within a relatively narrow range of 0.708–0.715, with ~ 50 % of recorded data clustering between 0.709 and 0.711 (Bataille et al., 2020). In stark contrast, our study reveals an extraordinary range of $^{87}\text{Sr}/^{86}\text{Sr}$ ratios, spanning from 0.71096 to 0.81720, with significant contributions from diverse geological provinces, sampling sites, and even tree genera. These variations far exceed those reported in other regions, highlighting the Amazon Forest as a region of exceptional isotopic heterogeneity. This extraordinary variability offers the potential for highly distinctive provenance, enabling precise tracking of ecological and biogeochemical processes across diverse geological and environmental settings within the Amazon. Such remarkable isotopic diversity underscores the uniqueness of the Amazon's geochemistry and its profound implications for ecological and environmental research.

4.2. Local $^{87}\text{Sr}/^{86}\text{Sr}$ variability

Local variability was low in sampling areas with uniform geology, such as the Cenozoic Trough of the Central Amazon region (Fig. 2). In contrast, variability was high in sampling areas with less uniform

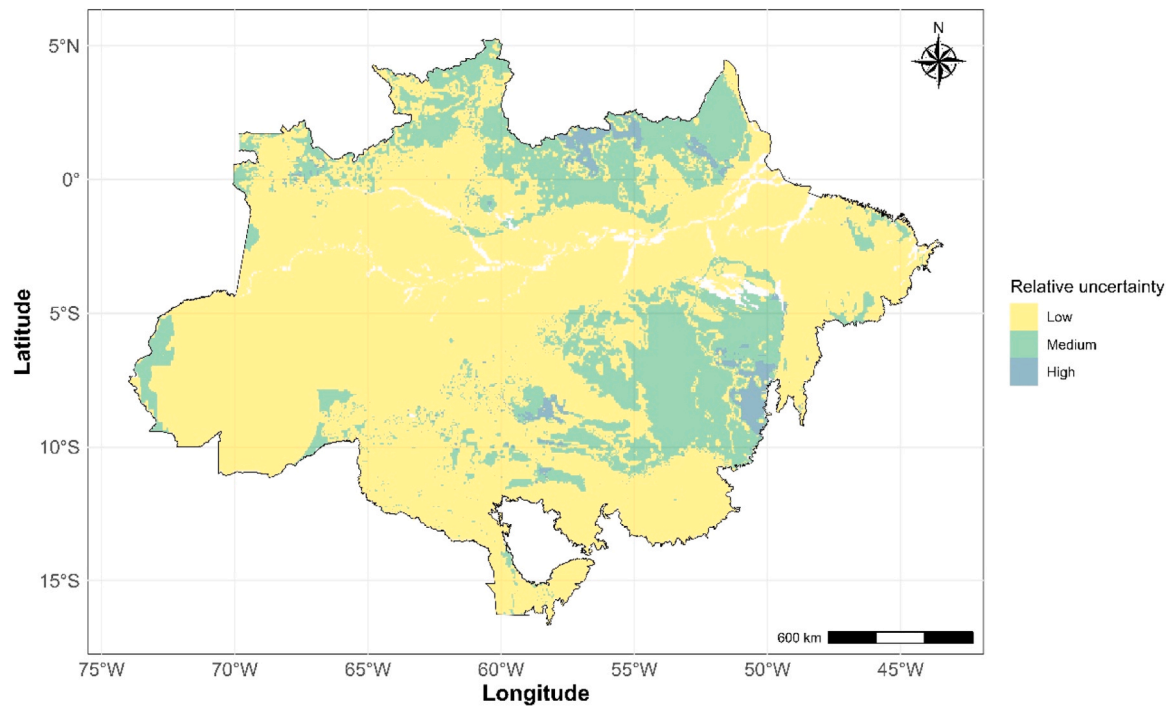


Fig. 9. Difference between the predicted $^{87}\text{Sr}/^{86}\text{Sr}$ ratio in tree wood by Kriging and Random Forest. Difference was categorized in three levels: low, medium and high.

geology, particularly in border zones between the Precambrian Shields (Brazilian and Guianas) and between these Shields and the Cenozoic terrain (Fig. 2).

These observations suggest two main conclusions. First, geology is the primary driver of the $^{87}\text{Sr}/^{86}\text{Sr}$ ratio in Amazon regions with uniform geology. Atmospheric deposition and preferential weathering seems to be not strong enough to override predominant geological control. As a result, within geologically uniform areas, the $^{87}\text{Sr}/^{86}\text{Sr}$ ratio may not serve as the best tracer due to its low variability. Consequently, a high sampling density is not necessary in such areas. Second, in regions with more complex geology, $^{87}\text{Sr}/^{86}\text{Sr}$ ratio can vary significantly over short distances, as observed in Rondonópolis (Fig. 1). In these $^{87}\text{Sr}/^{86}\text{Sr}$ ratio can serve as a powerful tracer of provenance, even over small spatial scales that encompass sharp geological contrasts. However, the sampling density in such areas should align with geological complexity to accurately map small-scale variations.

4.3. Geology as the main predictor and climatic as secondary predictors of $^{87}\text{Sr}/^{86}\text{Sr}$ ratios in trees

Some of our statistical results, including our GLM analysis and random forest, confirm that geology is the dominant control of wood $^{87}\text{Sr}/^{86}\text{Sr}$ ratios across the Amazon Forest (Figs. 8 and 9). High $^{87}\text{Sr}/^{86}\text{Sr}$ ratios are found in older rock units from the Pre-Cambrian Shields to the north (Guiana) and the south (Brazilian). In contrast, lower $^{87}\text{Sr}/^{86}\text{Sr}$ ratios dominate in younger Cenozoic sediments from the Andes deposited across the Central Amazon area (Fig. 1). These results are in line with the findings of Silva et al., (2023), who worked in part of the Amazon region with $^{87}\text{Sr}/^{86}\text{Sr}$ ratios of igneous and sedimentary rocks, unconsolidated soils, and sediments.

Although we have a small data set, the strong effect of rock age and $^{87}\text{Sr}/^{86}\text{Sr}$ ratio in wood aligns with previous studies showing that the $^{87}\text{Sr}/^{86}\text{Sr}$ ratio in ligneous plants is closely related to the underlying bedrock, whereas herbaceous plants or local animals tend to be more influenced by atmospheric deposition (Hartman and Richards, 2014). Moreover, although the Amazon region may no longer be entirely pristine, it remains relatively untouched compared to heavily cultivated

areas that undergo extensive soil amendment (Hoogewerff et al., 2019). Thus, our isoscape likely reflects a 'pristine' landscape described by Holt et al., (2021) reinforcing the reliability of $^{87}\text{Sr}/^{86}\text{Sr}$ isoscape modeling in this region.

In the random forest model, atmospheric vapor pressure (VPD), and air relative humidity (RH) were also identified as an important secondary control of wood $^{87}\text{Sr}/^{86}\text{Sr}$ ratios. Areas, characterized by Cenozoic sediments with low VPD and high RH, typical of the western Amazon had lower $^{87}\text{Sr}/^{86}\text{Sr}$ ratios (see VPD and RH map – Figure S3). The highest $^{87}\text{Sr}/^{86}\text{Sr}$ ratios were found in regions high VPD and low RH (Fig. 7), roughly corresponding to the southeastern Amazon, where the Brazilian Shield dominates (Fig. 1). While some of those relationships might be related to the coincidence of climate patterns with geology, we believe they represent a mechanistic process reflecting changes in weathering intensity. In regions of the Brazilian Shield characterized by high temperature, intermediate to high VPD (drier), and relatively flat topography, soils tend to be thick and highly weathered due to the interplay of low erosion rates and high weathering rates (Palmer and Edmond, 1992). These soils have developed over ancient Precambrian bedrock, resulting in a wide range of $^{87}\text{Sr}/^{86}\text{Sr}$ ratios in their mineral components. This variability arises because minerals in the original rock have distinct $^{87}\text{Rb}/^{86}\text{Sr}$ ratios at the time of formation (Capo et al., 1998). Over geological timescales, the decay of ^{87}Rb causes these ratios to diverge further (Bayon et al., 2022). During the weathering process, mineral phases with lower $^{87}\text{Sr}/^{86}\text{Sr}$ ratios, such as trace calcite and plagioclase, tend to weather more rapidly than those with higher $^{87}\text{Sr}/^{86}\text{Sr}$ ratios, such as biotite (Capo et al., 1998). As the soil matures, the depletion of minerals with low $^{87}\text{Sr}/^{86}\text{Sr}$ ratios leaves behind primary and secondary minerals with higher $^{87}\text{Sr}/^{86}\text{Sr}$ ratios, causing an overall increase in the bulk soil ratio (Capo et al., 1998). This effect of weathering intensity is particularly pronounced in tropical areas with low erosion rates, where soils can develop and age over extended periods (Quesada et al., 2011).

4.4. Sampling density limitations

Low sample density poses challenges in constructing isoscapes, as

highlighted by Makarewicz and Sealy, (2015), since sparse sampling may overlook the intricate variability of complex terrains. Low sampling density is also problematic when using machine-learning approaches such as random forest because they are very poor at extrapolating in areas with environmental conditions different from the training set (Bataille et al., 2020). Despite the limited sampling density, our study shows that $^{87}\text{Sr}/^{86}\text{Sr}$ in wood can be well-predicted because it is dominantly controlled by geology. We successfully developed wood $^{87}\text{Sr}/^{86}\text{Sr}$ ratio isoscapes using Random Forest and found stronger performance (Figs. 6 and 8). Although the Kriging model had a strong performance, the overall low uniformity of the standard deviations and the issues mentioned before with the semivariogram suggest that more samples are needed if one chooses to follow using Kriging spatial interpolation.

However, it is also clear that our current model has high remaining uncertainties since the normalized MAE and RMSE were near 10 %, indicated by a “rule of thumb” just a moderate to good performance and probably fails to capture many of the $^{87}\text{Sr}/^{86}\text{Sr}$ variations across the Amazon area due to the geological complexity of this region and the very low sampling density. An example is the fact that although we use the Cressie-Hawkins robust estimator to decrease the effects of outliers, we still observed some potential outliers and some variability in the semi-variance at larger distances (Figure S1). This indicates that we do not have enough samples to capture the spatial structure of our data or that spatial interpolation based on Euclidean distances may not be adequate to map the spatial variability of bioavailable $^{87}\text{Sr}/^{86}\text{Sr}$.

4.5. Certify timber origin using $^{87}\text{Sr}/^{86}\text{Sr}$ ratios

Even with a few samples, we successfully captured a broad spatial variability controlled by large-scale geological features (Shields vs. Cenozoic Through), suggesting that with increased sampling, and more accurate model $^{87}\text{Sr}/^{86}\text{Sr}$ ratios can be used for provenancing wood across the Amazon Forest. However, the lack of variability in $^{87}\text{Sr}/^{86}\text{Sr}$ ratios within the Amazon Through poses a challenge to distinguish the provenance of the sample coming from this region as evidenced by the low CV of $^{87}\text{Sr}/^{86}\text{Sr}$ ratios in areas like Atalaia, Jurua, ZF2, Itacoatiara, Maués, Tapajós, Monte Alegre and Flona Paru (Fig. 1 and 2). In such areas, other isotopes, like carbon, oxygen or sulfur, would be required to provide more precise provenance information. On the other hand, tracking provenance for wood from the Precambrian Shields presents a different challenge. This area is extremely geologically varied with a large range of $^{87}\text{Sr}/^{86}\text{Sr}$ in wood (Fig. 3). Even trees grown within a few kilometers appear to have large $^{87}\text{Sr}/^{86}\text{Sr}$ variations due to the high geological heterogeneity (Britton et al., 2020). Different species within the same site might even show some high variance because differential weathering processes in soil leads to distinct $^{87}\text{Sr}/^{86}\text{Sr}$ within the soil profile that are transmitted to trees based on their rooting depth (Capo et al., 1998). As noted by Holt et al., (2021), in geologically complex areas, plants may experience point bias, where a single plant's $^{87}\text{Sr}/^{86}\text{Sr}$ may not represent the broader area (Fig. 2). Notable examples in this work include samples from São Gabriel da Cachoeira and Rorainópolis in the Guiana Shield and Alta Floresta in the Brazilian Shield (Fig. 2).

This highlights the need to sample several specimens in these areas to achieve a more accurate spatial representation (Britton et al., 2020). Increasing sampling density could help capture subtle variations in the geological substrate, enhancing the reliability of the isoscapes and reducing model uncertainty. However, sampling in the Brazilian Shield presents several logistical challenges. First, this region has the highest deforestation rates in the Amazon, making it challenging to locate extensive forested areas for sampling. Second, the area is prone to violence related to land disputes and drug trafficking, which further complicates access to the remaining forest fragments.

4.6. Using $^{87}\text{Sr}/^{86}\text{Sr}$ provenance in other organisms in the Amazon region

Finally, we would like to call attention to the fact that the isoscapes

presented here, coupled with the significant $^{87}\text{Sr}/^{86}\text{Sr}$ variability, hold significant potential for diverse applications, as plants are the base of the food chain and serve as the primary source of strontium for animals and humans (Montgomery, 2010). The $^{87}\text{Sr}/^{86}\text{Sr}$ isoscapes developed here could play a pivotal role in addressing illegal plant and wildlife trafficking from the Amazon by determining the geographic origin and movement patterns of terrestrial and aquatic animals (e.g., Hegg et al., 2015b). For example, when traffickers claim that animals originate from specific breeding facilities, the $^{87}\text{Sr}/^{86}\text{Sr}$ ratios of the animals can be analyzed to verify their claims, as animals from the same facility should exhibit consistent isotopic signatures. Similarly, if a protected plant species was poached from the wild to serve as an ornamental plant, measuring the $^{87}\text{Sr}/^{86}\text{Sr}$ ratios along the wood profile should provide evidence of poaching, as has been demonstrated for cycads in South Africa (Retief et al., 2014).

The isoscapes also offer a valuable tool for understanding human history in the Amazon, particularly pre-Columbian civilizations (e.g., Laffoon et al., 2017). Or history of indigenous people enslavement during pre-Columbian and European periods (Chanca et al., 2021). For example, $^{87}\text{Sr}/^{86}\text{Sr}$ ratios could be useful for understanding the mobility of humans between settlements recently discovered using LIDAR technology (Iriarte et al., 2020; Neves, 2022; Rostain et al., 2024).

5. Conclusion

This study underscores the potential of the $^{87}\text{Sr}/^{86}\text{Sr}$ as a reliable method for tracing the geographic origin of timber in the Amazon, offering a valuable tool to combat illegal logging. The predictive power of the isoscapes developed here demonstrates the viability of this approach, particularly in regions with pronounced geological contrasts. However, challenges such as high intra-site variability in Precambrian cratons and limited isotopic resolution in parts of the Amazon highlight the need for additional sampling and methodological refinement. Addressing these gaps will not only enhance the accuracy and applicability of Sr isoscapes but also strengthen their role in supporting law enforcement efforts and promoting sustainable management of the Amazon's resources.

CRedit authorship contribution statement

N Higuchi: Writing – review & editing. **AC Barbosa:** Writing – review & editing. **A Brunello:** Writing – review & editing, Data curation. **M Tommasiello Filho:** Writing – review & editing. **CP Bataille:** Writing – review & editing, Data curation. **F Costa:** Writing – review & editing, Data curation. **GB Nardoto:** Writing – review & editing, Data curation. **LA Martinelli:** Writing – original draft, Supervision, Data curation, Conceptualization. **Araújo MG S:** Writing – review & editing, Data curation. **AL Abdalla Filho:** Writing – review & editing. **Gama Batista Ana Claudia:** Writing – review & editing. **IM Souza-Silva:** Writing – review & editing, Data curation.

Funding

This work was funded by the CAPES funding agency (Academic Cooperation Program in Public Security and Forensic Sciences – PRO-CAD), by INCT – CNPq (Forensic Metrology and Traceability in Agro-Environmental Quality – MRFor), and by The Nature Conservancy Brazil (TNC), in partnership with Google.

Recommendations

To enhance efforts against illegal logging in the Amazon, we recommend integrating $^{87}\text{Sr}/^{86}\text{Sr}$ isoscapes into existing timber traceability systems, such as Brazil's Forest Origin Document (DOF), to independently verify wood provenance. Expanding the Sr isotope dataset, particularly in geologically complex regions, will improve the

accuracy of provenance assessments. Interdisciplinary applications, including the combination of Sr isoscapes with other isotopic and genetic markers, can further strengthen forensic investigations and aid in combating wildlife trafficking. Standardized protocols for sample collection, processing, and analysis should be established to ensure methodological consistency, alongside the development of a centralized database of Amazonian Sr isotope signatures accessible to enforcement agencies. Lastly, incorporating Sr isotope analysis into timber certification frameworks and regulatory policies will reinforce environmental governance, enhance traceability, and support sustainable forest management in the Amazon.

Declaration of Competing Interest

The authors declare that they have no known competing financial interests or personal relationships that could have appeared to influence the work reported in this paper.

Acknowledgments

This work was supported by the Forest Management – INPA, the Dendrochronology Laboratory – UFLA, and the Wood Anatomy and Identification Laboratory – ESALQ, to whom we express our gratitude for donation the wood sample. We also thank Aparecido Candido Siqueira, a technical the Wood Anatomy and Identification Laboratory – ESALQ, for his technical support in sample preparation. Our appreciation extends to the technicians at the Isotopic Ecology Laboratory – CENA/USP: Fabiana C. Fracassi Adorno, Gustavo Gobert Baldi, and Isadora S. Ottani, for their support in analytical processing. Finally, we extend our gratitude to all other collaborators at the Isotopic Ecology Laboratory who contributed in any way to the completion of this project.

Appendix A. Supporting information

Supplementary data associated with this article can be found in the online version at [doi:10.1016/j.foreco.2025.122963](https://doi.org/10.1016/j.foreco.2025.122963).

Data availability

Data will be made available on request.

References

- Armaroli, E., Nilsson, A., Berglund, B., Sjögren, K.-G., 2024. Spatial ecology of moose in Sweden: Combined Sr-O-C isotope analyses of bone and antler. *PLoS One* 19, e0300867. <https://doi.org/10.1371/journal.pone.0300867>.
- Bataille, C.P., Bowen, G.J., 2012. Mapping $^{87}\text{Sr}/^{86}\text{Sr}$ variations in bedrock and water for large scale provenance studies. *Chem. Geol.* 304305 39–52. <https://doi.org/10.1016/j.chemgeo.2012.01.028>.
- Bataille, C.P., Crowley, B.E., Wooller, M.J., Bowen, G.J., 2020. Advances in global bioavailable strontium isoscapes. *Palaeogeogr. Palaeoclim. Palaeoecol.* 555, 109849. <https://doi.org/10.1016/j.palaeo.2020.109849>.
- Bataille, C.P., Jaouen, K., Milano, S., Trost, M., Steinbrenner, S., Crubézy, É., Colleter, R., 2021. Triple sulfur-oxygen-strontium isotopes probabilistic geographic assignment of archaeological remains using a novel sulfur isotope of western Europe. *PLoS One* 16, e0250383. <https://doi.org/10.1371/journal.pone.0250383>.
- Bayon, G., Bindeman, I.N., Trinquier, A., Retallack, G.J., Bekker, A., 2022. Long-term evolution of terrestrial weathering and its link to Earth's oxygenation. *Earth Planet. Sci. Lett.* 584, 117490. <https://doi.org/10.1016/j.epsl.2022.117490>.
- Brancalion, P.H.S., de Almeida, D.R.A., Vidal, E., Molin, P.G., Sontag, V.E., Souza, S.E.X. F., Schulze, M.D., 2018. Fake legal logging in the Brazilian Amazon. *Sci. Adv.* 4, e0250383. <https://doi.org/10.1126/sciadv.aat1192>.
- Britton, K., Le Corre, M., Willmes, M., Moffat, I., Grün, R., Mannino, M.A., Woodward, S., Jaouen, K., 2020. Sampling plants and malacofauna in $^{87}\text{Sr}/^{86}\text{Sr}$ bioavailability studies: implications for isotope mapping and reconstructing of past mobility patterns. *Front. Ecol. Evol.* 8. <https://doi.org/10.3389/fevo.2020.579473>.
- Capo, R.C., Stewart, B.W., Chadwick, O.A., 1998. Strontium isotopes as tracers of ecosystem processes: theory and methods. *Geoderma* 82, 197–225. [https://doi.org/10.1016/S0016-7061\(97\)00102-X](https://doi.org/10.1016/S0016-7061(97)00102-X).
- Chanca, I., Borges, C., Colanese, A.C., Macario, K., Toso, A., Fontanals-Coll, M., Anjos, R. dos, Muniz, M., Pereira, R., Talamo, S., Milheira, R.G., 2021. Food and diet of the pre-Columbian mound builders of the Patos Lagoon region in southern Brazil with stable isotope analysis. *J. Archaeol. Sci.* 133, 105439. <https://doi.org/10.1016/j.jas.2021.105439>.
- Costa, V.O.B., Koehler, H.S., Robert, R.C.G., 2024. Characterization of technical and legal irregularities in management plans in the Brazilian Amazon. *Trees For. People* 16, 100548. <https://doi.org/10.1016/j.tfp.2024.100548>.
- Cressie, N., Hawkins, D.M., 1980. Robust estimation of the variogram: I. *J. Int. Assoc. Math. Geol.* 12, 115–125. <https://doi.org/10.1007/BF01035243>.
- D'Andrea, R., Corona, C., Poszwa, A., Belingard, C., Domínguez-Delmás, M., Stoffel, M., Crivellaro, A., Crouzevialle, R., Cerbelaud, F., Costa, G., Paradis-Grenouillet, S., 2023. Combining conventional tree-ring measurements with wood anatomy and strontium isotope analyses enables dendroprovenancing at the local scale. *Sci. Total Environ.* 858, 159887. <https://doi.org/10.1016/j.scitotenv.2022.159887>.
- Dormontt, E.E., Boner, M., Braun, B., Breulmann, G., Degen, B., Espinoza, E., Gardner, S., Guillery, P., Hermanson, J.C., Koch, G., Lee, S.L., Kanashiro, M., Rimbawanto, A., Thomas, D., Wiedenhoeft, A.C., Yin, Y., Zahnen, J., Lowe, A.J., 2015. Forensic timber identification: It's time to integrate disciplines to combat illegal logging. *Biol. Conserv.* 191, 790–798. <https://doi.org/10.1016/j.biocon.2015.06.038>.
- Evans, J.A., Montgomery, J., Wildman, G., Boulton, N., 2010. Spatial variations in biosphere $^{87}\text{Sr}/^{86}\text{Sr}$ in Britain. *J. Geol. Soc. Lond.* 167, 1–4. <https://doi.org/10.1144/0016-76492009-090>.
- FATF, 2021. URL. Money Laundering from Environmental Crimes [WWW Document]. (<https://www.fatf-gafi.org/publications/methodsandtrends/documents/money-laundering-environmentalcrimes.html>) (accessed 1.27.25).
- Franca, C.S.S., Persson, U.M., Carvalho, T., Lentini, M., 2023. Quantifying timber illegality risk in the Brazilian forest frontier. *Nat. Sustain.* 6, 1485–1495. <https://doi.org/10.1038/s41893-023-01189-3>.
- Gaillardet, J., Dupre, B., Allegre, C.J., Négrel, P., 1997. Chemical and physical denudation in the Amazon River Basin. *Chem. Geol.* 142, 141–173. [https://doi.org/10.1016/S0009-2541\(97\)00074-0](https://doi.org/10.1016/S0009-2541(97)00074-0).
- van Geldern, R., Joachimski, M.M., Day, J., Jansen, U., Alvarez, F., Yolkin, E.A., Ma, X.-P., 2006. Carbon, oxygen and strontium isotope records of Devonian brachiopod shell calcite. *Palaeogeogr. Palaeoclim. Palaeoecol.* 240, 47–67. <https://doi.org/10.1016/j.palaeo.2006.03.045>.
- Genuer, R., Poggi, J.-M., Tuleau-Malot, C., 2015. VSURF: an R package for variable selection using random forests. *R. J.* 7, 19. <https://doi.org/10.32614/RJ-2015-018>.
- Gori, Y., Stradiotti, A., Camin, F., 2018. Timber isoscapes. A case study in a mountain area in the Italian Alps. *PLoS One* 13, e0192970. <https://doi.org/10.1371/journal.pone.0192970>.
- Greenwell, B.M., 2017. pdp: An R Package for Constructing Partial Dependence Plots.
- Haji, F., Poszwa, A., Bouchez, J., Guérol, F., 2017. Radiogenic and “stable” strontium isotopes in provenance studies: a review and first results on archaeological wood from shipwrecks. *J. Archaeol. Sci.* 86, 24–49. <https://doi.org/10.1016/j.jas.2017.09.005>.
- Hartman, G., Richards, M., 2014. Mapping and defining sources of variability in bioavailable strontium isotope ratios in the Eastern Mediterranean. *Geochim. Cosmochim. Acta* 126, 250–264. <https://doi.org/10.1016/j.gca.2013.11.015>.
- Hegg, J.C., Giarrizzo, T., Kennedy, B.P., 2015a. Diverse early life-history strategies in migratory Amazonian catfish: implications for conservation and management. *PLoS One* 10, e0129697. <https://doi.org/10.1371/journal.pone.0129697>.
- Hegg, J.C., Giarrizzo, T., Kennedy, B.P., 2015b. Diverse early life-history strategies in migratory Amazonian catfish: implications for conservation and management. *PLoS One* 10, e0129697. <https://doi.org/10.1371/journal.pone.0129697>.
- Hengl, T., Heuvelink, G.B.M., Rossiter, D.G., 2007. About regression-kriging: from equations to case studies. *Comput. Geosci.* 33, 1301–1315. <https://doi.org/10.1016/j.cageo.2007.05.001>.
- Hiemstra, P.H., Pebesma, E.J., Twenhöfel, C.J.W., Heuvelink, G.B.M., 2009. Real-time automatic interpolation of ambient gamma dose rates from the Dutch radioactivity monitoring network. *Comput. Geosci.* 35, 1711–1721. <https://doi.org/10.1016/j.cageo.2008.10.011>.
- Holt, E., Evans, J.A., Madgwick, R., 2021. Strontium ($^{87}\text{Sr}/^{86}\text{Sr}$) mapping: a critical review of methods and approaches. *Earth Sci. Rev.* 216, 103593. <https://doi.org/10.1016/j.earscirev.2021.103593>.
- Hoogewerff, J.A., Reimann, Clemens, Ueckermann, H., Frei, R., Frei, K.M., van Aswegen, T., Stirling, C., Reid, M., Clayton, A., Ladenberger, A., Albanese, S., Andersson, M., Baritz, R., Batista, M.J., Bel-lan, A., Birke, M., Cicchella, D., Demetriades, A., De Vivo, B., De Vos, W., Dinelli, E., Duriš, M., Dusza-Dobek, A., Eggen, O.A., Eklund, M., Ernsten, V., Filzmoser, P., Flight, D.M.A., Forrester, S., Fuchs, M., Fügedi, U., Gilucis, A., Gregorauskiene, V., De Groot, W., Gulán, A., Halamić, J., Haslinger, E., Hayoz, P., Hoffmann, R., Hrvatovic, H., Husnjak, S., Janik, L., Jordan, G., Kaminari, M., Kirby, J., Kivisilla, J., Klos, V., Krone, F., Kwečko, F., Kutí, L., Lima, A., Locutura, J., Lucivjansky, D.P., Mann, A., Mackovych, D., Matschullat, J., McLaughlin, M., Malýuk, B.I., Maquil, R., Meuli, R. G., Mol, G., Negrel, P., Connor, O., Oorts, R.K., Ottesen, R.T., Pasieczna, A., Petersell, W., Pfeiderer, S., Poňavič, M., Pramuka, S., Prazeres, C., Rauch, U., Radusinović, S., Reimann, C., Sadeghi, M., Salpeteur, I., Scanlon, R., Schedl, A., Scheib, A.J., Schoeters, I., Šefčík, P., Sellersjö, E., Skopljak, F., Slaninka, I., Soriano-Disla, J.M., Šorsá, A., Srivkora, R., Staffilov, T., Tarvainen, T., Trendavilov, V., Valera, P., Verougstraete, V., Vidojević, D., Zissimos, A., Zomeni, Z., 2019. Bioavailable $^{87}\text{Sr}/^{86}\text{Sr}$ in European soils: a baseline for provenancing studies. *Sci. Total Environ.* 672, 1033–1044. <https://doi.org/10.1016/j.scitotenv.2019.03.387>.
- Hothorn, T., Hornik, K., Zeileis, A., 2006. Unbiased recursive partitioning: a conditional inference framework. *J. Comput. Graph. Stat.* 15, 651–674. <https://doi.org/10.1198/106186006X133933>.
- 2019 Interpol, 2019. Global Forestry Enforcement: Strengthening law enforcement cooperation against forestry crime [WWW Document]. Interpol. URL <https://www.interpol.int/2019/03/20/Global-Forestry-Enforcement-Strengthening-law-enforcement-cooperation-against-forestry-crime>

- www.interpol.int/content/download/5149/file/Global%20Forestry%20Enforcement%20Prospectus%202019-web.pdf. (accessed 1.27.25).
- Iriarte, J., Robinson, M., de Souza, J., Damasceno, A., da Silva, F., Nakahara, F., Ranzi, A., Aragao, L., 2020. Geometry by design: contribution of lidar to the understanding of settlement patterns of the mound villages in SW Amazonia. *J. Comput. Appl. Archaeol.* 3, 151–169. <https://doi.org/10.5334/jcaa.45>.
- Kafino, C.V., de Sousa, I.M.C., Barbieri, C.B., de Amorim, A.M., Santos, R.V., 2024. A proof-of-concept study: Determining the geographical origin of Brazilwood, (*Paubrasilia echinata*) with the use of strontium isotopic fingerprinting. *Sci. Justice* 64, 159–165. <https://doi.org/10.1016/j.scijus.2023.12.006>.
- Kuhn, M., 2008. Building Predictive Models in R Using the **caret** Package. *J. Stat. Softw.* 28. <https://doi.org/10.18637/jss.v028.i05>.
- Ladegaard-Pedersen, P., Achilleos, M., Dörflinger, G., Frei, R., Kristiansen, K., Frei, K.M., 2020. A strontium isotope baseline of Cyprus. Assessing the use of soil leachates, plants, groundwater and surface water as proxies for the local range of bioavailable strontium isotope composition. *Sci. Total Environ.* 708, 134714. <https://doi.org/10.1016/j.scitotenv.2019.134714>.
- Laffoon, J.E., Sonnemann, T.F., Shafie, T., Hofman, C.L., Brandes, U., Davies, G.R., 2017. Investigating human geographic origins using dual-isotope ($^{87}\text{Sr}/^{86}\text{Sr}$, $\delta^{18}\text{O}$) assignment approaches. *PLoS One* 12, e0172562. <https://doi.org/10.1371/journal.pone.0172562>.
- Lapola, D.M., Pinho, P., Barlow, J., Aragão, L.E.O.C., Berenguer, E., Carmenta, R., Liddy, H.M., Seixas, H., Silva, C.V.J., Silva-Junior, C.H.L., Alencar, A.A.C., Anderson, L.O., Armenteras, D., Brovkin, V., Calders, K., Chambers, J., Chini, L., Costa, M.H., Faria, B.L., Fearnside, P.M., Ferreira, J., Gatti, L., Gutierrez-Velez, V.H., Han, Z., Hibbard, K., Koven, C., Lawrence, P., Pongratz, J., Portela, B.T.T., Rounsevell, M., Ruane, A.C., Schaldach, R., da Silva, S.S., von Randow, C., Walker, W.S., 2023. The drivers and impacts of Amazon forest degradation. *Science* 379, 1979. <https://doi.org/10.1126/science.abp8622>.
- 1997 IGooverts, 1997. Geoestatística para avaliação de recursos naturais. Geoestatística para avaliação de recursos naturais. Oxford University Press, Oxford.
- Low, M.C., Schmitz, N., Boeschoten, L.E., Cabezas, J.A., Cramm, M., Haag, V., Koch, G., Meyer-Sand, B.R.V., Paredes-Villanueva, K., Price, E., Thornhill, A.H., Van Brusselen, J., Zuidema, P.A., Deklerck, V., Dormontt, E.E., Shapcott, A., Lowe, A.J., 2022. Tracing the world's timber: the status of scientific verification technologies for species and origin identification. *IAWA J.* 44, 63–84. <https://doi.org/10.1163/22941932-bja10097>.
- Lugli, F., Cipriani, A., Bruno, L., Ronchetti, F., Cavazzuti, C., Benazzi, S., 2022. A strontium isotope of Italy for provenance studies. *Chem. Geol.* 587, 120624. <https://doi.org/10.1016/j.chemgeo.2021.120624>.
- Ma, C., Vander Zanden, H.B., Wunder, M.B., Bowen, G.J., 2020. `<scp>assignR</scp>`: An `<scp>r</scp>` package for isotope-based geographic assignment. *Methods Ecol. Evol.* 11, 996–1001. <https://doi.org/10.1111/2041-210X.13426>.
- Makarewicz, C.A., Sealy, J., 2015. Dietary reconstruction, mobility, and the analysis of ancient skeletal tissues: expanding the prospects of stable isotope research in archaeology. *J. Archaeol. Sci.* 56, 146–158. <https://doi.org/10.1016/j.jas.2015.02.035>.
- MMA, 2016. Normative Instruction No. 9. Ministério do Meio Ambiente, Brasil.
- Montgomery, J., 2010. Passports from the past: investigating human dispersals using strontium isotope analysis of tooth enamel. *Ann. Hum. Biol.* 37, 325–346. <https://doi.org/10.3109/03014461003649297>.
- Neves, E.G., 2022. Sob os tempos do equinócio: Oito mil anos de história na Amazônia central. Ubu.
- Palmer, M.R., Edmond, J.M., 1992. Controls over the strontium isotope composition of river water. *Geochim. Cosmochim. Acta* 56, 2099–2111. [https://doi.org/10.1016/0016-7037\(92\)90332-D](https://doi.org/10.1016/0016-7037(92)90332-D).
- Quesada, C.A., Lloyd, J., Anderson, L.O., Fyllas, N.M., Schwarz, M., Czimczik, C.I., 2011. Soils of Amazonia with particular reference to the RAINFOR sites. *Biogeosciences* 8, 1415–1440. <https://doi.org/10.5194/bg-8-1415-2011>.
- Retief, K., West, A.G., Pfab, M.F., 2014. Can stable isotopes and radiocarbon dating provide a forensic solution for curbing illegal harvesting of threatened cycads? *J. Forensic Sci.* 59, 1541–1551. <https://doi.org/10.1111/1556-4029.12644>.
- Reynolds, A.C., Betancourt, J.L., Quade, J., Jonathan Patchett, P., Dean, J.S., Stein, J., 2005. $^{87}\text{Sr}/^{86}\text{Sr}$ sourcing of ponderosa pine used in Anasazi great house construction at Chaco Canyon, New Mexico. *J. Archaeol. Sci.* 32, 1061–1075. <https://doi.org/10.1016/j.jas.2005.01.016>.
- Rostain, S., Dorison, A., de Saulieu, G., Prümers, H., Le Pennec, J.-L., Mejía Mejía, F., Freire, A.M., Pagán-Jiménez, J.R., Descola, P., 2024. Two thousand years of garden urbanism in the Upper Amazon. *Science* 383 (1979), 183–189. <https://doi.org/10.1126/science.adf6317>.
- Santos, R.V., Sondag, F., Cochonneau, G., Lagane, C., Brunet, P., Hattingh, K., Chaves, J. G.S., 2015. Source area and seasonal $^{87}\text{Sr}/^{86}\text{Sr}$ variations in rivers of the Amazon basin. *Hydrol. Process* 29, 187–197. <https://doi.org/10.1002/hyp.10131>.
- Silva, C., dos Santos, E.A., Dussin, I.A., Montibeller, C.C., de Avelar Las Casas Rebelo, V., da Costa Pereira Laval Heilbron, M., Pimentel, L.C.G., Landau, L., 2023. Spatial distribution of strontium and neodymium isotopes in South America: a summary for provenance research. *Environ. Earth Sci.* 82, 348. <https://doi.org/10.1007/s12665-023-11028-5>.
- Snoeck, C., Ryan, S., Pouncett, J., Pellegrini, M., Claeys, P., Wainwright, A.N., Mattioli, N., Lee-Thorp, J.A., Schulting, R.J., 2020. Towards a biologically available strontium isotope baseline for Ireland. *Sci. Total Environ.* 712, 136248. <https://doi.org/10.1016/j.scitotenv.2019.136248>.
- Vlam, M., Smith, B., Oliveira, L.F., Johnson, R., Silva, R., 2025. Evaluating the potential of oxygen isoscapes for tropical timber tracing. *For. Ecol. Manag.* 590, 122757. <https://doi.org/10.1016/j.foreco.2025.122757>.
- Wang, X., Bocksberger, G., Arandjelovic, M., Agbor, A., Angedakin, S., Aubert, F., Ayimisin, E.A., Bailey, E., Barubiyo, D., Bessone, M., Bobe, R., Bonnet, M., Boucher, R., Brazzola, G., Brewer, S., Lee, K.C., Carvalho, S., Chancellor, R., Cipoletta, C., Cohen, H., Copeland, S.R., Corogenes, K., Costa, A.M., Coupland, C., Curran, B., de Ruiter, D.J., Deschner, T., Dieguez, P., Dierks, K., Dilambaka, E., Dowd, D., Dunn, A., Egbe, V.E., Finckh, M., Fruth, B., Gijanto, L., Yuh, Y.G., Goedmakers, A., Gokee, C., Gomes Coelho, R., Goodman, A.H., Granjon, A.-C., Grimes, V., Grueter, C.C., Haour, A., Hedwig, D., Hermans, V., Hernandez-Aguilar, R. A., Hohmann, G., Imong, I., Jeffery, K.J., Jones, S., Junker, J., Kadam, P., Kambere, M., Kambi, M., Kienast, I., Knudson, K.J., Langergraber, K.E., Lapeyre, V., Lapuente, J., Larson, B., Lautenschläger, T., le Roux, P., Leinert, V., Llana, M., Logan, A., Lowry, B., Lüdecke, T., Maretti, G., Marrocoli, S., Fernandez, R., McNeill, P.J., Meier, A.C., Meller, P., Monroe, J.C., Morgan, D., Mulindahabi, F., Murai, M., Neil, E., Nicholl, S., Niyigaba, P., Normand, E., Ormsby, L.J., Diotoh, O., Pacheco, L., Piel, A., Preece, J., Regnaut, S., Richard, F.G., Richards, M.P., Rundus, A., Sanz, C., Sommer, V., Sponheimer, M., Steele, T.E., Stewart, F.A., Tagg, N., Tédonzong, L.R., Tickle, A., Toubga, L., van Schijndel, J., Vergnes, V., Njomen, N.W., Wessling, E.G., Willie, J., Wittig, R.M., Yurkiw, K., Zipkin, A.M., Zuberbühler, K., Kühl, H.S., Boesch, C., Oelze, V.M., 2024. Strontium isotope of sub-Saharan Africa allows tracing origins of victims of the transatlantic slave trade. *Nat. Commun.* 15, 10891. <https://doi.org/10.1038/s41467-024-55256-0>.
- Watkinson, C., Gasson, P., Rees, G., Boner, M., 2020. The development and use of isoscapes to determine the geographical origin of *Quercus* spp. in the United States. *Forests* 11, 862. <https://doi.org/10.3390/f11080862>.
- Willmes, M., Bataille, C.P., James, H.F., Moffat, I., Mc Morrow, L., Kinsley, L., Armstrong, R.A., Eggins, S., Grün, R., 2018. Mapping of bioavailable strontium isotope ratios in France for archaeological provenance studies. *Appl. Geochem.* 90, 75–86. <https://doi.org/10.1016/j.apgeochem.2017.12.025>.
- Wright, M.N., Ziegler, A., 2017. ranger: a fast implementation of random forests for high dimensional data in C++ and R. *J. Stat. Softw.* 77. <https://doi.org/10.18637/jss.v077.i01>.